DOI: 10.26599/FSHW.2024.9250188

Y.F. Chen et al. / Food Science and Human Wellness 14 (2025)

Contents lists available at SciOpen

Food Science and Human Wellness

journal homepage: https://www.sciopen.com/journal/2097-0765

A highly sensitive electrochemical sensing platform based on Zn-$CuGaO_2$@CMK-3 signal amplification for simultaneous detection of the sunset yellow and tartrazine in foods

Yongfeng Chen[1,#], Rui Gao[1,#], Yufeng Sun[1], Ruiqiang Wang[2], Geoffrey I.N. Waterhouse[3], Xuguang Qiao[1], Zhixiang Xu[1*]

[1]*College of Food Science and Engineering, Shandong Agricultural University, Tai'an 271018, People's Republic of China*

[2]*Shandong Cayon Testing Co., LTD., Jining 272000, People's Republic of China*

[3]*School of Chemical Sciences, The University of Auckland, Auckland 1142, New Zealand*

ABSTRACT: In this work, a highly sensitive electrochemical sensor based on Zn-doped copper gallium oxide@ordered mesoporous carbon (Zn-$CuGaO_2$@CMK-3) for signal amplification was successfully developed for the simultaneous detection of sunset yellow (SY) and tartrazine (TZ) in foods. Compared with $CuGaO_2$@CMK-3, Zn-$CuGaO_2$@CMK-3 offered enhanced conductivity and catalytic properties owing to the improved carrier density, which was beneficial to the electrooxidation of SY and TZ. Under the optimal testing conditions, the constructed Zn-$CuGaO_2$@CMK-3/GCE sensor offered a wide linear concentration range (0.25 to 100.00 μmol/L) for the detection of both SY and TZ. The limits of detection for SY and TZ were 0.044 μmol/L and 0.059 μmol/L, respectively. Recovery experiments were performed in milk, white vinegar and biscuit samples, yielding satisfactory recoveries (82.70%-114.80%). Furthermore, the sensor was successfully applied to the determination of the SY and TZ residues in two kinds of carbonated drinks, and the results were nearly consistent with those detected by the high performance liquid chromatography (HPLC) method ($P > 0.05$).

Keywords: Zn-doped copper gallium oxide; Ordered mesoporous carbon; Electrochemical sensor; Sunset yellow; Tartrazine

1. Introduction

Sunset yellow (SY) and tartrazine (TZ) are widely used in the manufacture of cakes, candies, jams and beverages due to their bright colors, good water solubility, high stability and low cost[1-3]. However, due to the presence of azo functional groups (-N=N-) in these synthetic dyes, excessive consumption of SY and TZ can have negative effects on human health (including anxiety, allergies, eczema and migraines)[4]. Rrecently, various methods have been used for the detection of SY and TZ, including high performance liquid chromatography (HPLC)[5], liquid chromatography/tandem mass spectrometry[6] and capillary electrophoresis[7]. These methods offer accuracy, though require skilled operators, long analysis times and expensive instruments[8-13]. Electrochemical sensors offer many advantages over these traditional detection

[#]Rui Gao and Yongfeng Chen contributed equally to this work.
***Corresponding author**
zhixiangxu@sina.com (Zhixiang Xu)

Received 28 October 2023
Received in revised from 29 December 2023
Accepted 16 February 2024

techniques for the detection of target analytes in foods, including a fast response time, low capital costs and simplicity[14-15]. To date, a series of nanomaterials-based electrochemical sensors have been reported for the detection of SY and TZ, such as Au/PEDOT/MWCNT-CONH-UIO-66/GCE[16], MIG-CuS@COOH-MWCNTs/GCE[17], PDA/NiS@HCS/GCE[3], However, they are unable to achieve the simultaneous detection of SY and TZ. Though the ePAD[18] and Cu-BTC/CPE[4] sensors can realize the simultaneous detection of SY and TZ, their limits of detection (LOD) are higher and their linear ranges are narrower. Since SY and TZ are commonly present together in foods, establishing a sensitive electrochemical sensing platform for the simultaneous detection of SY and TZ is of practical importance.

Delafossite copper gallium oxide ($CuGaO_2$), a p-type transparent semiconductor with a wide band gap (~3.6 eV), attracts great interest in the fields of solar cells[19], photocatalyst[20] and electrocatalyst[21] due to its simple preparation, low cost and high chemical stability. Numerous studies have shown that divalent cation doping is an effective strategy for improving the electrical conductivity of $CuGaO_2$[22]. Doping with Zn^{2+}, which has a similar ionic radius to the host cations, enhances the electrical conductivity whilst minimizing lattice distortions[23, 24]. Accordingly, Zn^{2+}-doped $CuGaO_2$ (Zn-$CuGaO_2$) is a promising material for electrochemical sensor development. However, Zn-$CuGaO_2$ nanoparticles show a tendency to aggregate. This problem can be overcome by compositing Zn-$CuGaO_2$ with ordered mesoporous carbons possessing high conductivity and large specific surface area, such as CMK-3[25-27]. CMK-3 is a suitable substrate for the in-situ growth of Zn-$CuGaO_2$. Moreover, the large pore structure of CMK-3 can effectively shorten the distance between the analyte to the electrode surface, thus improving the detection efficiency[28]. Hence, Zn-$CuGaO_2$@CMK-3 composites were expected to offer good performance in the construction of an electrochemical sensing platform for the simultaneous detection of SY and TZ.

Herein, a one-pot hydrothermal method was applied to synthesize Zn-$CuGaO_2$@CMK-3 composites with good catalytic properties and excellent electron transfer capability. Deposition of Zn-$CuGaO_2$@CMK-3 onto a glassy carbon electrode (GCE) delivered a Zn-$CuGaO_2$@CMK-3/GCE electrochemical sensing platform for the simultaneous detection of SY and TZ. The electrochemical performance of Zn-$CuGaO_2$@CMK-3-GCE sensor was then systematically evaluated through cyclic voltammetry (CV) and square wave voltammetry (SWV) measurements. Furthermore, experiments established that the anti-interference, reproducibility, repeatability and stability of the constructed sensor were all satisfactory for SY and TZ quantification. This study demonstrates a simple and sensitive strategy for the simultaneous quantification of SY and TZ in foods.

2. Experimental section

2.1 Materials and reagents

Milk, white vinegar, biscuit and two kinds of carbonated drinks were purchased from a local supermarket in Tai'an (Shandong, China).

Sunset yellow (SY), $Ga(NO_3)_3 \cdot xH_2O$ and polyamide were supplied by Macklin Biochemical Tech. Co., Ltd. (Shanghai, China). Tartrazine (TZ) was supplied by Aladdin Industrial Corporation (Shanghai, China).

$Cu(NO_3)_2·3H_2O$ and $Zn(NO_3)_2·6H_2O$ were purchased from Tianjin Kemio Chemical Reagent Co., Ltd. (Tianjin, China). CMK-3 was obtained from Nanjing XFNANO Materials Tech. Co., Ltd. (Nanjing, China). L-lysine was obtained from Solarbio Biotechnology Co., Ltd. (Beijing, China). Glucose, $CaCl_2$, $MgSO_4$, $(CH_3COO)_2Zn$ and Na_2CO_3 were purchased from Tianjin Kaitong Chemical Reagent Co., Ltd. (Tianjin, China). Double-distilled water (DDW, 18.2 MΩ cm^{-1}) was used in all experiments and obtained from an Aike ultrapure water instrument (Chengdu, China).

2.2 Instruments and apparatus

A CHI650E electrochemical workstation connected to a standard three-electrode system (Shanghai, China) was employed for all electrochemical experiments. A glassy carbon electrode with different surface modifications served as the working electrode, a platinum electrode was used as the auxiliary electrode and a saturated calomel electrode used as the reference electrode. Scanning electron microscopy (SEM) images were acquired on a ZEISS Crossbeam 540 microscope (Carl Zeiss Microscopy GmbH, Germany). X-ray diffraction (XRD) patterns were collected on a Bruker D8 Advance. Energy dispersive spectroscopy (EDS) images were determined using a Zeiss Gemini (Sigma 500 VP) instrument. Fourier transform infrared (FT-IR) spectra were recorded on a NICOLET iS10 Spectrometer (Thermo Fisher, USA).

A HPLC system, comprising a C_{18} reversed-phase column (4.6 mm × 250 mm, 5 μm), two LC-10ATVP pumps and a SPD-10AVP UV detector, was applied for the detection of SY and TZ (254 nm, Shimadzu, Kyoto, Japan). The mobile phase was ammonium acetate aqueous solution (0.02 mol L^{-1})/methanol with a gradient elution.

2.3 Synthesis of $CuGaO_2$, Zn-$CuGaO_2$ and Zn-$CuGaO_2$@CMK-3

The Zn-$CuGaO_2$@CMK-3 composite was synthesized according to a literature method with a minor modification[29]. Briefly, 0.50 mmol $Ga(NO_3)_3·xH_2O$, 0.50 mmol $Cu(NO_3)_2·3H_2O$, 0.20 mmol $Zn(NO_3)_2·6H_2O$ and 30.00 mg of CMK-3 were added to a solvent mixture containing 12.00 mL of DDW, 8.00 mL of ethylene glycol and 6.00 mL of an KOH aqueous solution (1.00 M). After stirring in an ice bath for 1 h, the resulting dispersion was transferred to a 100.0 mL autoclave and heated at 200 ℃ for 24 h. Finally, the product was collected by centrifugation (3996×g, 10 min), then washed successively with 10.0 wt.% ammonia, 10.0 wt.% HNO_3 solution and repeatedly with DDW.

Zn-$CuGaO_2$, $CuGaO_2$@CMK-3, and $CuGaO_2$ were prepared in the same way as Zn-$CuGaO_2$@CMK-3, except that CMK-3, $Zn(NO_3)_2·6H_2O$, or CMK-3 and $Zn(NO_3)_2·6H_2O$, respectively, were not added during the syntheses.

2.4 Construction of the Zn-$CuGaO_2$@CMK-3/GCE sensor

Prior to modification, the bare GCE was firstly polished with an Al_2O_3 slurry and washed with DDW and ethanol under ultrasonication to achieve a mirror finish (potential difference was no more than 90 mV). Next, 1.50 mg of the Zn-$CuGaO_2$@CMK-3 nanocomposite was dispersed to 1.00 mL of a chitosan acetic acid solution (0.01 wt.%). Then, 9.00 μL Zn-$CuGaO_2$@CMK-3 suspension was dripped onto the surface of the

GCE followed by natural drying of the modified electrode at room temperature (to produce the Zn-$CuGaO_2$@CMK-3/GCE). The fabrication procedure of the Zn-$CuGaO_2$@CMK-3/GCE is depicted in Scheme 1.

2.5 Sample pretreatment

SY and TZ recovery experiments were performed in milk, biscuit and white vinegar samples to evaluate the accuracy of the Zn-$CuGaO_2$@CMK-3/GCE sensor. Briefly, 10.00 mL of the milk or vinegar samples or 1.00 g of the biscuit sample dispersed in 10.00 mL DDW and 1.00 mL of mixed SY and TZ standard solution (containing SY and TZ at concentrations of 5.00 μmol/L, 25.00 μmol/L, 50.00 μmol/L or 100.00 μmol/L) were transferred to a 100 mL beaker and the resulting mixtures ultrasonicated for 20 min to remove any dissolved CO_2. The sample solutions were then incubated for 5 h, after which their pH was adjusted to 6.0 by adding a citric acid solution (200.00 g L^{-1}). After heating to 60 °C, 1.00 g of a polyamide slurry was poured into the samples under stirring for a short time. The obtained mixtures were then filtered through a G3 vertical melting funnel and the collected solid was washed with DDW (60 °C, pH 4.0) and methanol-formic acid mixed solution for 3 to 5 times. Then the collected mixture was washed to neutral with DDW, after which the SY and TZ desorbed with an ethanol-ammonium-DDW mixed solution until all the pigment was completely desorbed. The elution solution was collected, neutralized with acetic acid and then evaporated to near dryness. Finally, the SY and TZ residues were re-dissolved in 5.00 mL PBS and analyzed using the fabricated sensor.

The two kinds of carbonated drinks were pretreated in accordance with the above procedure, but without the addition of the mixed SY and TZ standard solution. The SY and TZ contents in the extracts were determined using the Zn-$CuGaO_2$@CMK-3 sensor and a HPLC method.

3. Results and discussion

3.1 Characterization of Zn-$CuGaO_2$ and Zn-$CuGaO_2$@CMK-3

Scanning electron microscopy was used to investigate the surface morphologies of Zn-$CuGaO_2$ and Zn-$CuGaO_2$@CMK-3. Zn-$CuGaO_2$ consisted of loose aggregates of small spherical particles (Fig. 1a), with individual particle sizes being approximately 20-30 nm. For Zn-$CuGaO_2$@CMK-3, as illustrated in Fig. 1b, small Zn-$CuGaO_2$ nanoparticles could be seen uniformly distributed over the mesh-like CMK-3 support.

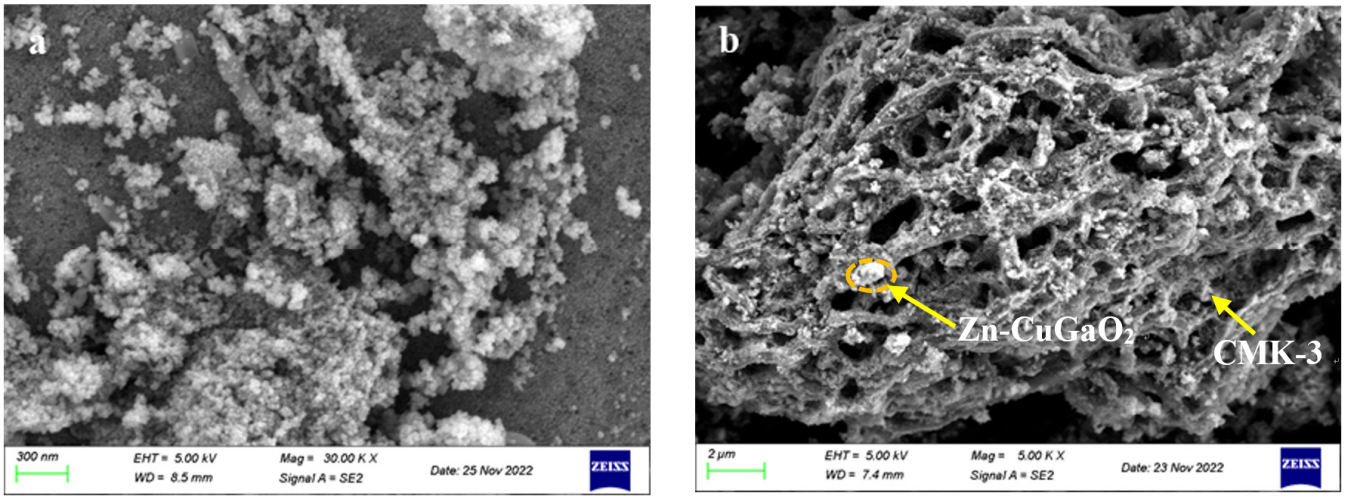

Fig. 1 SEM images of (a) Zn-$CuGaO_2$ and (b) Zn-$CuGaO_2$@CMK-3.

Powder XRD was used to examine the crystallinity and phases present in $CuGaO_2$, Zn-$CuGaO_2$, CMK-3 and Zn-$CuGaO_2$@CMK-3 (Fig. 2a). The XRD pattern for $CuGaO_2$ showed peaks at 15.40°, 31.20°, 36.18°, 44.62°, 55.60° and 62.26°, which were readily indexed to the (003), (006), (012), (015), (018) and (110) reflections, respectively, of $CuGaO_2$[30]. The diffraction pattern for Zn-$CuGaO_2$ showed similar peaks to $CuGaO_2$, indicating that Zn doping did not alter the bulk crystal structure. However, the intensities of the (006) and (110) peaks for Zn-$CuGaO_2$ were much weaker compared to $CuGaO_2$, suggesting a possible change in exposed crystal faces with Zn doping. CMK-3 showed a broad XRD peaks at 24.80°, corresponding to the (002) plane of graphite[31]. The XRD pattern for Zn-$CuGaO_2$@CMK-3 contained contributions from both Zn-$CuGaO_2$ and CMK-3, confirming the successful synthesis of a Zn-$CuGaO_2$@CMK-3 composite. Next, the particle sizes and zeta potentials of $CuGaO_2$ and Zn-$CuGaO_2$ were measured to investigate the effect of the doping of Zn on $CuGaO_2$. As shown in Fig. 2b and Fig. 2c, the average particle size of Zn-$CuGaO_2$ (712.31 nm ± 1.12 nm) was smaller than that of $CuGaO_2$ (1280 nm ± 1.78 nm), indicating the addition of Zn made $CuGaO_2$ smaller and more uniform. The result demonstrated that Zn-$CuGaO_2$ possessed a larger specific surface area compared to $CuGaO_2$, thus providing more binding sites for the analytes. Compared with $CuGaO_2$ (+26.03 mV), the zeta potential of Zn-$CuGaO_2$ was more positive (+34.34 mV), which was conducive to the adsorption of negatively charged targets. The EDS spectrum of Zn-$CuGaO_2$@CMK-3 showed the presence of Zn, Cu, Ga, O and C (with the carbon being from the CMK-3 support) (Fig. 3a-f), further confirming the successful formation of a Zn-$CuGaO_2$@CMK-3 nanocomposite.

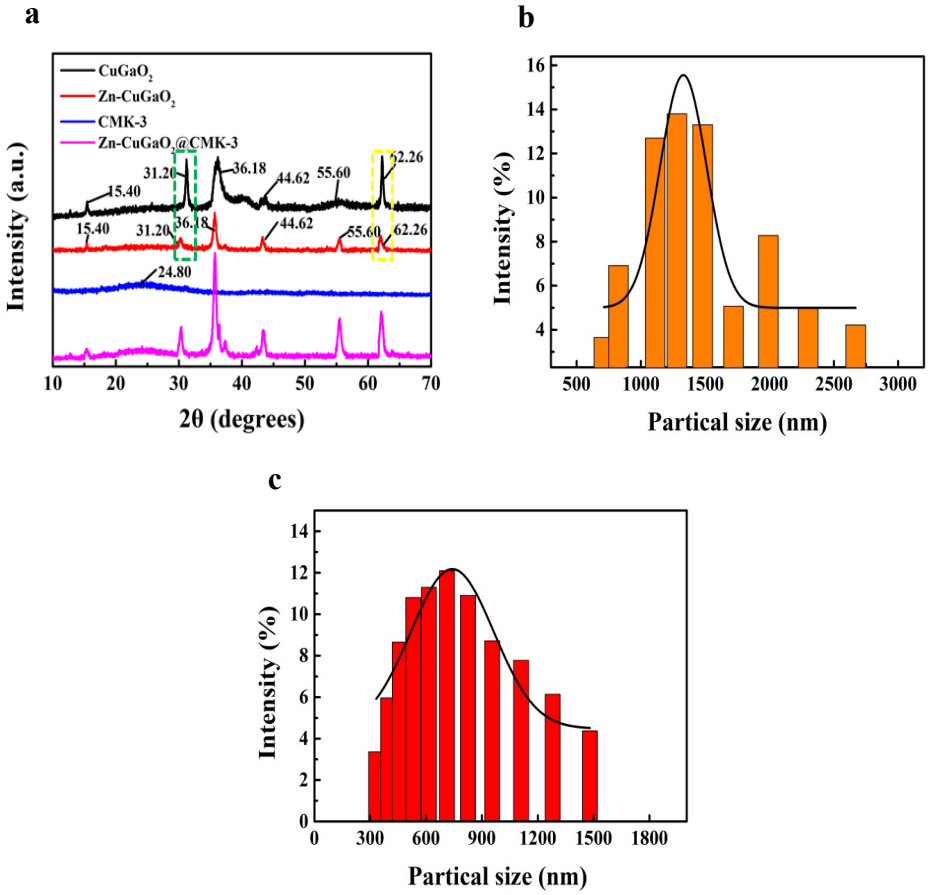

Fig. 2 (a) XRD patterns of $CuGaO_2$, Zn-$CuGaO_2$, CMK-3 and Zn-$CuGaO_2$@CMK-3. Size distributions of the (b) $CuGaO_2$ and (c) Zn-$CuGaO_2$.

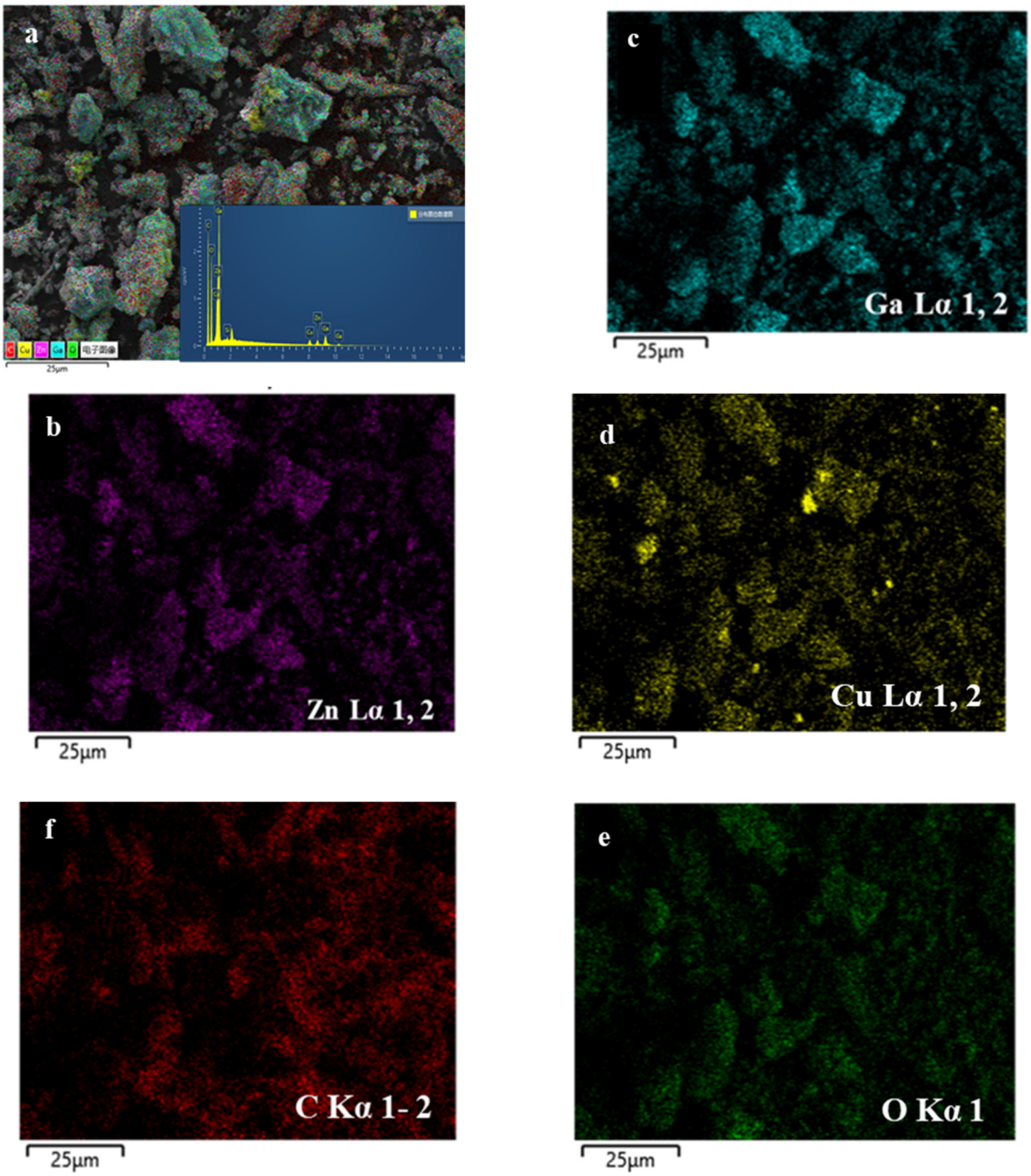

Fig. 3 EDS elemental mapping images of (a) all elements (combined), (b) Zn, (c) Ga, (d) Cu, (e) O and (f) C for Zn-$CuGaO_2$@CMK-3.

3.2 Electrochemical characterization studies on different modified electrodes

Electrochemical impedance spectroscopy (EIS) data were collected for the GCE and modified GCEs to evaluate their interfacial properties. Experiments were performed in a 5.00 mmol/L $[Fe(CN)_6]^{3/4-}$ solution (Fig. 4a). The charge transfer resistance (R_{ct}), double layer capacitance (C_{dl}), solution resistance (R_s) and Warburg impedance (Z_w) were calculated from the Randles equivalent-circuit model (inset in Fig. 4a). Zn-$CuGaO_2$/GCE possessed a higher R_{ct} (763.12 Ω) than the bare GCE (124.58 Ω), which is explained by the low electrical conductivity of Zn-$CuGaO_2$. Conversely, $CuGaO_2$@CMK-3/GCE exhibited a low R_{ct} (14.80 Ω), which can be attributed to the excellent electrical conductivity and electron transfer ability of the CMK-3 support. The R_{ct} of Zn-$CuGaO_2$@CMK-3/GCE (10.33 Ω) was the lowest amongst the electrodes tested,

confirming the Zn^{2+}-doping of $CuGaO_2$ boosted the electron transfer rate. Results validate the use of Zn-$CuGaO_2$ and CMK-3 in the design of an electrochemical sensor for SY and TZ.

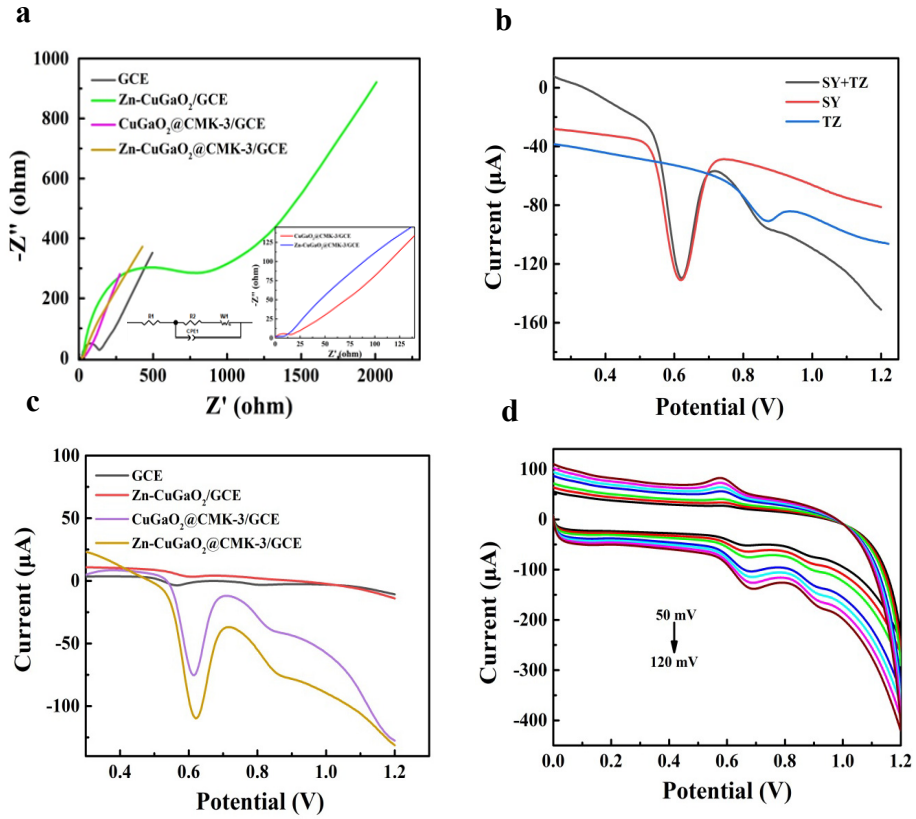

Fig. 4 (a) EIS plots for GCE, Zn-$CuGaO_2$/GCE, $CuGaO_2$@CMK-3/GCE and Zn-$CuGaO_2$@CMK-3/GCE in 5.00 mmol/L $[Fe(CN)_6]^{3/4-}$ solution containing 0.10 M KCl. (b) SWV curves of Zn-$CuGaO_2$@CMK-3/GCE in the presence of 100.00 μmol/L SY or/and 100.00 μmol/L TZ solution in PBS (pH 7.0). (c) SWV responses of bare GCE, Zn-$CuGaO_2$/GCE, $CuGaO_2$@CMK-3/GCE and Zn-$CuGaO_2$@CMK-3/GCE in a 100.00 μmol/L SY and 100.00 μmol/L TZ solution. (d) CV plots for Zn-$CuGaO_2$@CMK-3/GCE in a 100.00 μmol/L SY and 100.00 μmol/L TZ solution at different scan rates from 50 to 120 mV s^{-1}.

Fig. 4b shows SWV plots for Zn-$CuGaO_2$@CMK-3/GCE in PBS (pH 7.0) containing 100.00 μmol/L SY and/or 100.00 μmol/L TZ. In a 100.00 μmol/L SY solution, an oxidation peak was observed at +0.620 V, associated with the oxidation of the -OH group in the SY molecule. For TZ (100.00 μmol/L), an oxidation peak was seen at +0.852 V due to oxidation of the -OH group in TZ. In a PBS solution containing both SY and TZ (each 100.00 μmol/L), two distinct oxidation peaks were observed at +0.620 V and +0.852 V, consistent with the oxidation of SY and TZ, respectively. The result confirmed that the Zn-$CuGaO_2$@CMK-3/GCE was appropriate for the individual or simultaneous detection of SY and TZ. SWV was next applied to study the electrochemical behaviors of the GCE, Zn-$CuGaO_2$/GCE, $CuGaO_2$@CMK-3/GCE and Zn-$CuGaO_2$@CMK-3/GCE in a solution containing 100.00 μmol/L SY and 100.00 μmol/L TZ (Fig. 4c). The oxidation peaks of SY and TZ appeared at +0.564 V and +0.816 V on the bare GCE, with the peak currents of 4.728 μA and 1.592 μA, respectively. For Zn-$CuGaO_2$/GCE, the SWV responses towards SY and TZ were lower than that on the bare GCE due to the poor electron transfer properties of Zn-$CuGaO_2$. After the GCE was modified with $CuGaO_2$@CMK-3, the SWV currents for both SY and TZ increased whilst the peak potentials shifted negatively, which is explained by $CuGaO_2$@CMK-3 catalyzing the oxidation of SY and TZ. For

Zn-$CuGaO_2$@CMK-3/GCE, the electrooxidation currents of SY (88.06 μA) and TZ (13.18 μA) were 18.63 times and 8.28 higher, respectively, compared to the GCE. Further, the peak potentials for both SY and TZ oxidation were shifted in more negative direction compared with $CuGaO_2$@CMK-3/GCE (and also GCE), indicating that Zn-doping enhanced the electrocatalytic properties of Zn-$CuGaO_2$@CMK-3 for SY and TZ oxidation.

3.3 Electrochemical mechanism of SY and TZ oxidation on Zn-$CuGaO_2$@CMK-3/GCE

To study the electrochemical oxidation mechanism of SY and TZ on the Zn-$CuGaO_2$@CMK-3/GCE, CV responses were measured at different scan rates from 50 to 120 mV s^{-1} in PBS containing 100.00 μmol/L SY and 100.00 μmol/L TZ (Fig. 4d). As shown in Fig. S1a and Fig. S1b, good linear relationships were established between the peak current of SY and TZ and the scanning rate, with $Ip_{SY} = 0.6097\ \nu - 12.9280$ ($R^2 = 0.9974$) and $Ip_{TZ} = 1.8896\ \nu^{1/2} – 9.6593$ ($R^2 = 0.9960$), respectively, where ν represents the scanning rate. The results illustrated the electrochemical reaction kinetics of SY and TZ were controlled by adsorption and diffusion, respectively[31, 32]. Fig. S1c shows the SWV curves for SY and TZ in solutions of pH ranging from 5.0 to 9.0. The peak potential (Ep) for both SY and TZ shifted to more negative values as the pH increased. In Fig. S1d and Fig. S1e, linear relationships were established between the Ep for SY and TZ with pH, with Ep = -0.03210pH + 0.8457 ($R^2 = 0.9930$) for SY and Ep = -0.0281pH + 1.0729 ($R^2 = 0.9996$) for TZ. Results suggest that the ratio of electrons and protons involved in the electrooxidation processes of SY and TZ were both 2:1, consistent with previous literature reports[33, 34].

3.4 Optimization of testing conditions

The influence of Zn-$CuGaO_2$@CMK-3 dispersion concentration and volume on the SWV current of SY and TZ was investigated to improve the sensitivity of the Zn-$CuGaO_2$@CMK-3/GCE sensor for SY and TZ determination (Fig. S2a and Fig. S2b). The SWV peak current towards SY and TZ first increased and then decreased with increases in Zn-$CuGaO_2$@CMK-3 dispersion concentration and volume, with the highest peak currents recorded at 1.50 mg L^{-1} and 9.00 μL, respectively. Therefore, 9.00 μL of a 1.50 mg L^{-1} Zn-$CuGaO_2$@CMK-3 dispersion was used for sensor fabrication.

Fig. S2c shows the effect of the incubation time on the SWV current in PBS (pH 7.0) containing 100.00 μmol/L SY and 100.00 μmol/L TZ. The peak current of both SY and TZ increased continuously as the incubation time increased from 1 min to 4 min. After incubation for 4 min, the peak currents for SY and TZ plateaued, demonstrating the binding sites on Zn-$CuGaO_2$@CMK-3 to SY and TZ were close to saturation after 4 min. Accordingly, 4 min was selected as the optimal incubation time.

The pH of the electrolyte is a key factor affecting the analytical performance of the constructed sensor towards SY and TZ. In Fig. S2d, the SWV responses towards SY and TZ (100.00 μmol/L) first increased and then decreased as the pH range was increased from 5.0 to 9.0, reaching the maximum values at pH 7.0. These results can be explained by the fact that SY and TZ are both protic aromatic molecules, which are prone to deprotonation to form anions at high pH (pH > 7.0), thus resulting in electrostatic repulsion[35]. Consequently, PBS with a pH of 7.0 was used in subsequent experiments.

3.5 Simultaneous determination of SY and TZ with the Zn-CuGaO$_2$@CMK-3/GCE sensor

Under the optimal testing conditions, SWV curves were collected for the Zn-CuGaO$_2$@CMK-3/GCE sensor in PBS (pH 7.0) containing different concentrations of SY and TZ. Fig. 5a shows that the peak currents for both SY and TZ increased with concentration from 0.25 μmol/L to 100.00 μmol/L. Fig. 5b reveals a good linear relationship between the SWV response and SY concentration (Ip (-μA) = 0.9586C (μmol/L) + 0.3405, with R^2 = 0.9992). For TZ (Fig. 5c), a linear concentration dependence was also found, described by the equation Ip (-μA) = 0.1316C (μmol/L) + 0.3860 (R^2 = 0.9972). The LODs for SY and TZ were calculated to be 0.044 μmol/L and 0.059 μmol/L, respectively.

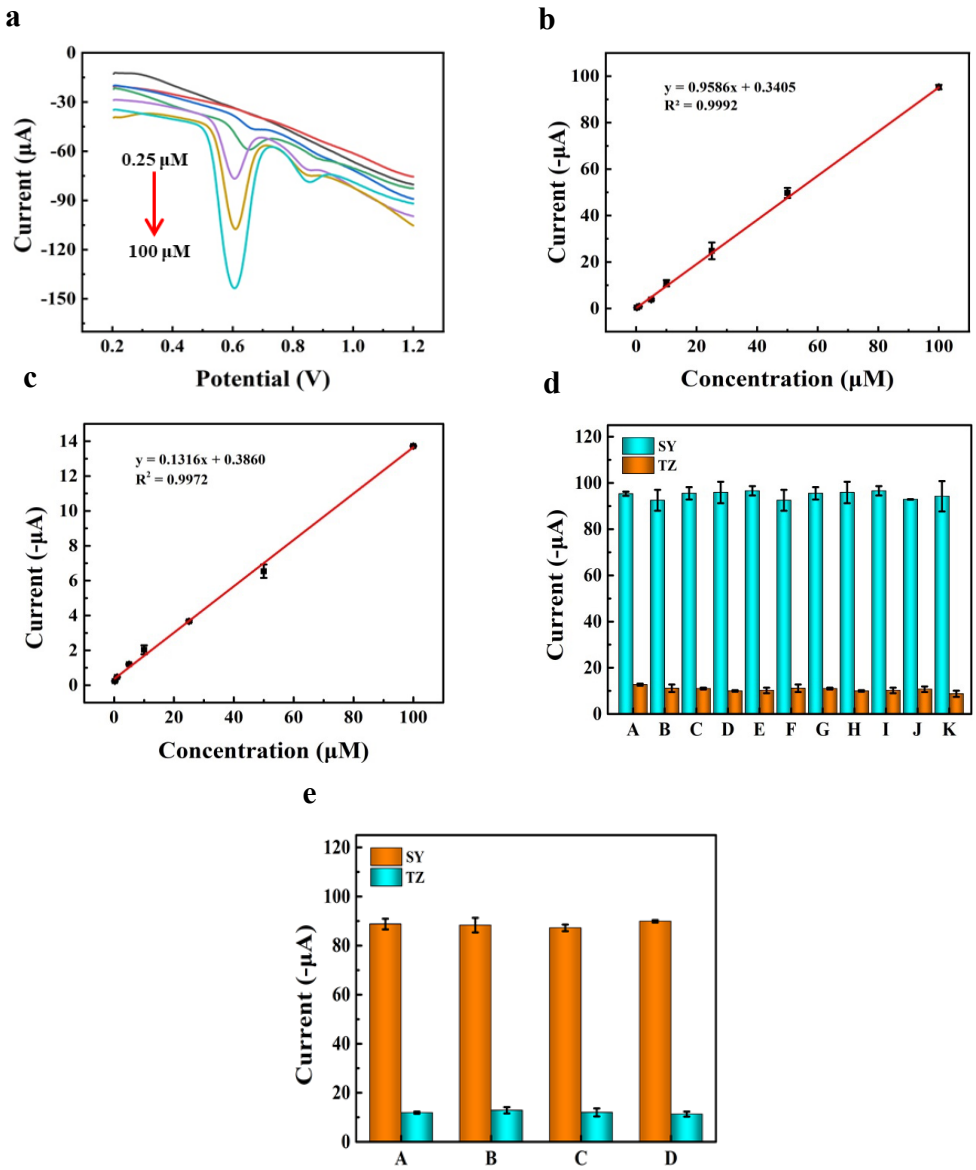

Fig. 5 (a) SWV responses of the Zn-CuGaO$_2$@CMK-3/GCE sensor in PBS (pH 7.0) containing various concentrations of SY and TZ in the range of 0.25-100.00 μmol/L (0.25 μmol/L, 1.00 μmol/L, 5.00 μmol/L, 10.00 μmol/L, 25.00 μmol/L, 50.00 μmol/L and 100.00 μmol/L under optimal conditions. (b) Corresponding linear relationship between the SWV peak current and the SY concentration from 0.25 to 100.00 μmol/L. (c) Corresponding linear relationship between the SWV peak current and the TZ concentration from 0.25 to 100.00 μmol/L. (d) Interference study data obtained by measuring the SWV current towards SY and TZ (100.00 μmol/L) in (A) absence, and presence of possible interferents. Possible interferents included a 100-fold higher concentration of (B) Ca^{2+}, (C) Mg^{2+}, (D) Zn^{2+}, (E) Na^{+}, (F) Cl^{-}, (G) SO_4^{2-}, (H) CH_3COO^{-}, (I) CO_3^{2-}, or a 10-fold higher concentration of (J) L-lysine or (K) glucose. (e) Interference study data obtained by measuring the SWV current towards SY and TZ (100.00 μmol/L) in (A) absence, and presence of common analogues. Common analogues included (B) Sudan I, (C) Ponceau 4R or (D) Allura Red at the same concentration.

Table S1 compares the analytical performance between the Zn-$CuGaO_2$@CMK-3/GCE sensor with previously reported analytical methods for the detection of SY and TZ. The LODs for SY and TZ determined using the Zn-$CuGaO_2$@CMK-3/GCE sensor were lower than most previously reported methods[36-42]. Although the LODs of the developed sensor towards SY and TZ detection were slightly higher than those of the ERGO-AuNRs/GCE sensor, P(*β*-CD/Arg)/CysA-AuNPs/AuE sensor and ZnO@Ag SERS sensor[43-45], the fabrication process of the Zn-$CuGaO_2$@CMK-3/GCE sensor was much simpler and cost-effective compared with those sensors. Moreover, the detection time of the proposed sensor was shorter and the linear range of the Zn-$CuGaO_2$@CMK-3/GCE sensor was wider than those of most methods[36-45], thus providing a promising strategy for the quantification of SY and TZ.

3.6 Anti-interference, reproducibility, repeatability and stability of the constructed sensor

The possible influence of matrix interference on the SWV responses of the Zn-$CuGaO_2$@CMK-3/GCE sensor towards SY and TZ were tested in presence of some small organic molecules (e.g. 10-fold higher concentration of L-lysine or glucose), inorganic ions (100-fold higher concentration of Ca^{2+}, Mg^{2+}, Zn^{2+}, Na^{+}, Cl^{-}, SO_4^{2-}, CH_3COO^{-} or CO_3^{2-}) and analogues (the same concentration of Sudan I, Ponceau 4R or Allura Red). As shown in Fig. 5d and Fig. 5e, the presence of the these molecules and ions had negligible effect on the peak currents of SY and TZ (RSD ≤ 6.52%), suggesting that the anti-interference performance of the Zn-$CuGaO_2$@CMK-3/GCE sensor was satisfactory.

Six Zn-$CuGaO_2$@CMK-3/GCE electrodes were prepared to evaluate the reproducibility of the constructed sensor for the simultaneous detection of SY and TZ under the optimal conditions (Fig. S3a). The Zn-$CuGaO_2$@CMK-3/GCE sensor had excellent reproducibility for SY and TZ detection, with relative standards deviations (RSDs) of 4.70% (SY) and 3.61% (TZ) for the 6 sensors. Furthermore, the repeatability of measurements using the Zn-$CuGaO_2$@CMK-3 sensors was explored by using a single modified electrode for six measurements under the same conditions in a solution containing 100.00 μmol/L SY and 100.00 μmol/L TZ (Fig. S3b). The RSDs were in the range of 1.89% to 2.83%, revealing that the repeatability of measurements using the developed sensor was acceptable. The storage stability of the developed sensor was examined over 30 days at 4℃ (Fig. S3c). After 30 days, the SWV peak currents of SY and TZ determined using the Zn-$CuGaO_2$@CMK-3/GCE sensor were 91.33% and 85.32%, respectively, of the original values. These results implied the fabricated sensor possessed good storage stability.

3.7 Trueness and applicability of the Zn-$CuGaO_2$@CMK-3/GCE sensor

To evaluate the trueness of the Zn-$CuGaO_2$@CMK-3/GCE sensor, recovery experiments using SY and TZ spiked milk, biscuit and white vinegar samples were conducted. Table 1 summarizes the experimental data. The recoveries of SY and TZ were in the range of 82.70%-114.80% with RSDs of 2.48%-6.56%, demonstrating the high accuracy of the prepared sensor.

The practicability of the fabricated sensor was verified by quantifying SY and TZ in two kinds of carbonated drinks using the Zn-$CuGaO_2$@CMK-3/GCE sensor and a HPLC method. The SY levels in the two kinds of carbonated drinks detected using the Zn-$CuGaO_2$@CMK-3/GCE sensor were (0.76 ± 1.21) mg kg^{-1}

and (7.07 ± 4.29) mg kg^{-1}, while the SY concentrations determined by the HPLC method were (0.69 ± 1.58) mg kg^{-1} and (6.77 ± 3.24) mg kg^{-1}, respectively. The TZ concentrations in the two kinds of carbonated drinks determined using the Zn-$CuGaO_2$@CMK-3/GCE sensor were (6.11 ± 2.05) mg kg^{-1} and (5.87 ± 4.97) mg kg^{-1}, while the levels determined by the HPLC method were (5.84 ± 4.18) mg kg^{-1} and (6.64 ± 2.58) mg kg^{-1} (Fig. S4), respectively. No significant difference was found between the SY and TZ contents measured using the two methods (Table S2), indicating the feasibility and reliability of the developed sensor for the simultaneous detection of SY and TZ in real samples.

4. Conclusion

A sensitive electrochemical sensor based on Zn-$CuGaO_2$@CMK-3/GCE for signal amplification was successfully constructed for the simultaneous quantification of SY and TZ in foods. The Zn-$CuGaO_2$@CMK-3 nanocomposite with excellent electron transfer capacity showed outstanding electrocatalytic property attributed to the doping of Zn, which was beneficial for the electrooxidation of SY and TZ. The Zn-$CuGaO_2$@CMK-3/GCE sensor offered a wide linear range and a low LOD for both SY and TZ. Furthermore, the constructed sensor possessed excellent sensitivity, repeatability, reproducibility and stability, and could readily be applied for the SY and TZ detection in actual samples (e.g. carbonated drinks). Results encourage the wider used of copper-based delafossite semiconductor materials, such as Zn-doped $CuGaO_2$, in the construction of electrochemical sensing platforms for the monitoring and quantification of toxic and hazardous organic compounds in foods.

Conflict of Interest Statement

We declare that we have no conflict of interest.

Acknowledgements

This work was financially supported by the Key R&D Program of Shandong Province, China (No. 2023CXGC010712). GINW acknowledges funding support from the MacDiarmid Institute for Advanced Materials and Nanotechnology.

References

[1] O.I. Lipskikh, E.I. Korotkova, Ye.P. Khristunova, J. Barek, B. Kratochvil, Sensors for voltammetric determination of food azo dyes-A critical review, Electrochim. Acta 260 (2018) 974-985. https://doi.org/10.1016/j.electacta.2017.12.027.

[2] X.L. Qiu, L.M. Lu, J. Leng, Y.F. Yu, W.M. Wang, M. Jiang, L. Bai, An enhanced electrochemical platform based on graphene oxide and multi-walled carbon nanotubes nanocomposite for sensitive determination of Sunset Yellow and Tartrazine, Food Chem. 190 (2016) 889-895. https://doi.org/10.1016/j.foodchem.2015.06.045.

[3] Y.F. Chen, G.I.N. Waterhouse, H.M. Sun, X.G. Qiao, Y.F. Sun, Z.X. Xu, Novel ratiometric electrochemical sensing platform with dual-functional poly-dopamine and NiS@HCS signal amplification for sunset yellow detection in foods, Food Chem. 390 (2022) 133193. https://doi.org/10.1016/j.foodchem.2022.133193.

[4] L.D. Ji, Q. Cheng, K.B. Wu, X.F. Yang, Cu-BTC frameworks-based electrochemical sensing platform for rapid and simple determination of Sunset yellow and Tartrazine, Sens. Actuators B Chem. 231 (2016) 12-17. https://doi.org/10.1016/j.snb.2016.03.012.

[5] A. Maria de Souza Santos Cheibub, E. Silva Bahiense de Lyra, B. Jardim Alves, A. Andrade Donagemma, A. Duarte Pereira Netto, Development and validation of a multipurpose and multicomponent method for the simultaneous determination of six synthetic dyes in different foodstuffs by HPLC-UV-DAD, Food Chem. 323 (2020) 126811. https://doi.org/10.1016/j.foodchem.2020.126811.

[6] C.F. Tsai, C.H. Kuo, D.Y.C. Shih, Determination of 20 synthetic dyes in chili powders and syrup-preserved fruits by liquid chromatography/tandem mass spectrometry, J. Food .Drug Anal. 23 (2015), 453-462. https://doi.org/10.1016/j.jfda.2014.09.003.

[7] F.J. Liu, C.T. Liu, W. Li, A.N. Tang, Dispersive solid-phase microextraction and capillary electrophoresis separation of food colorants in beverages using diamino moiety functionalized silica nanoparticles as both extractant and pseudostationary phase, Talanta 132 (2015) 366-372. https://doi.org/10.1016/j.talanta.2014.09.014.

[8] M. Li, Y. He, X. Ma, Separation and quantitative detection of fermentation γ-polyglutamic acid, J. Future Foods 2(1) (2022) 34-40. https://doi.org/10.1016/j.jfutfo.2022.03.015.

[9] B. Çapan, A. Bağdatli, Investigation of physicochemical, microbiological and sensorial properties for organic and conventional retail chicken meat, Food Sci. Hum. Well. 10 (2021) 183-190. https://doi.org/10.1016/j.fshw.2021.02.007.

[10] Y.W. Wang, B. Zhang, M.J. Guo, C.Y. Wang, Q.B. Wang, L.T. Zhang, Y. Zhang, Rapid detection of cordycepin in food by surface-enhanced Raman technique, J. Future Foods 3(1) (2023) 24-28. https://doi.org/10.1016/j.jfutfo.2022.09.004.

[11] D. Liang, Y.J. Xu, F. Peng, W. Ma, Y. Zhao, Plasmonic metal NP-bismuth composite film with amplified SERS activity for multiple detection of pesticides and veterinary drugs, Chem. Eng. J. 474 (2023) 145933. https://doi.org/10.1016/j.cej.2023.145933.

[12] Y. Zhao, Y.J. Xu, X.H. Jing, W. Ma, SERS-active plasmonic metal NP-CsPbX3 films for multiple veterinary drug residues detection, Food Chem. 412 (2023) 135420. https://doi.org/10.1016/j.foodchem.2023.135420.

[13] Y. Zhao, J.J. Shao, Z. Jin, W.W. Zheng, J. Yao, W. Ma, Plasmon-enhanced electroreduction activity of Au-AgPd Janus nanoparticles for ochratoxin a detection, Food Chem. 412 (2023) 135526. https://doi.org/10.1016/j.foodchem.2023.135526.

[14] Y.F. Sun, J.B. He, G.I.N. Waterhouse, L.H. Xu, H.Y. Zhang, X.G. Qiao, Z.X. Xu, A selective molecularly imprinted electrochemical sensor with GO@COF signal amplification for the simultaneous determination of sulfadiazine and acetaminophen, Sens. Actuators B Chem. 300 (2019) 126993. https://doi.org/10.1016/j.snb.2019.126993.

[15] G.B. Ning, Q.M. Duan, H. Liang, H.F. Liu, M. Zhou, C.L. Chen, C. Zhang, H. Zhao, C.P. Li, One stone two birds: electrochemical and colorimetric dual-mode biosensor based on copper peroxide/covalent organic framework nanocomposite for ultrasensentive norovirus detection, Food Sci. Hum. Well. 13(2) (2024) 920-931. https://doi.org/10.26599/FSHW.2022.9250079.

[16] J.H. Li, D.H. Zhu, H. Huang, S.Q. Xie, J.K. Xu, R.R. Yue, X.M. Duan, High-efficient electrochemical sensing platform based on MOF-doped Au/PEDOT composites toward simultaneous detection of catechin and sunset yellow in tea beverage, Electrochim. Acta 462 (2023) 142732. https://doi.org/10.1016/j.electacta.2023.142732.

[17] Y.F. Chen, Y.F. Sun, G.I.N. Waterhouse, H.J. Gao, Z.X. Xu, Highly selective molecularly imprinted gel-based electrochemical sensor with CuS@COOH-MWCNTs signal amplification for simultaneous detection of vanillin and tartrazine in foods, Sens. Actuators B Chem. 377 (2023) 133045. https://doi.org/10.1016/j.snb.2022.133045.

[18] G.F. Alves, L.V. de Faria, T.P. Lisboa, C.C. de Souza, B.L.M. Fernandes, M.A.C.Matos, R.C. Matos, A portable and affordable paper electrochemical platform for the simultaneous detection of sunset yellow and tartrazine in food beverages and desserts, Microchem. J. 181 (2022) 107799. https://doi.org/10.1016/j.microc.2022.107799.

[19] L. Chen, L.L. Qiu, H.J. Wang, Y.F. Yuan, L.X. Song, F.Q. Xie, J. Xiong, P.F. Du, $CuGaO_2$ Nanosheet Arrays as the Hole-Transport Layer in Inverted Perovskite Solar Cells, ACS Appl. Nano Mater. 5 (2022) 10055-10063. https://doi.org/10.1021/acsanm.3c00816.

[20] M. Choi, S. Yagi, Y. Ohta, K. Kido, T. Hayakawa, Estimation of delafossite p-type $CuGaO_2$/ZnO hybrids as semiconductor photocatalyst by controlling particle size, J. Phys. Chem. Solids 150 (2021) 109845. https://doi.org/10.1016/j.jpcs.2020.109845.

[21] H. Gao, M. Yang, X. Liu, X.L. Dai, X.Q. Bao, D.H. Xiong, Hydrothermal synthesized delafossite $CuGaO_2$ as an electrocatalyst for water oxidation, Front. Optoelectron. 15 (2022) 8. https://doi.org/10.1007/s12200-022-00014-7.

[22] C.Y. Tsay, C.L. Chen, Improved electrical properties of p-type $CuGaO_2$ semiconductor thin films through Mg and Zn doping, Ceram. Int. 43 (2017) 2563-2567. https://doi.org/10.1016/j.ceramint.2016.11.059.

[23] K. Meesombad, N. Sato, S. Pitiphattharabun, G. Panomsuwan, R. Techapiesancharoenkij, K. Surawathanawises, C. Wongchoosuk, S. Boonsalee, J.H. Pee, O. Jongprateep, Zn-doped TiO_2 nanoparticles for glutamate sensors, Ceram. Int. 47 (2021) 21099-21107. https://doi.org/10.1016/j.ceramint.2021.04.113.

[24] L. Li, Y.T. Xu, H.F. Hu, Y.Y. Jing, C.Y. Xu, H. Zhang, L. Jin, L.L. Shi, Y.G. Zou, X.H. Ma, Study on the optoelectronic properties of Zn and Mg doped $CuGaO_2$ nanoplates, Opt. Mater. 123 (2022) 111865. https://doi.org/10.1016/j.optmat.2021.111865.

[25] F.L. Lai, J.R. Feng, T. Heil, G.C. Wang, P. Adler, M. Antonietti, M. Oschatz, Strong metal oxide-support interactions in carbon/hematite nanohybrids activate novel energy storage modes for ionic liquid-based supercapacitors, Energy Storage Mater. 20 (2019) 188-195. https://doi.org/10.1016/j.ensm.2019.04.035.

[26] X.X. Li, M.X. Ma, W.R. Lv, G.H. Wu, R.Q. Lian, W.M. Zhang, Z.Y. Li, CMK-3 modified separator for ultra-high stability performance Cu1.8Se aluminum batteries, Nano Res. 15 (2022) 8136-8145. https://doi.org/10.1007/s12274-022-4517-x.

[27] R.P. Wu, Q. Ye, K. Wu, S.Y. Cheng, T.F. Kang, H.X. Dai, Adsorption performance of CMK-3 and C-FDU-15 in NO removal at low temperature, J. Environ. Sci. 87 (2020) 289-298. https://doi.org/10.1016/j.jes.2019.07.014.

[28] G.Z. Fang, G.Y. Liu, Y.K. Yang, S. Wang, Quartz crystal microbalance sensor based on molecularly imprinted polymer membrane and three-dimensional Au nanoparticles@mesoporous carbon CMK-3 functional composite for ultrasensitive and specific determination of citrinin, Sens. Actuators B Chem. 230 (2016) 272-280. https://doi.org/10.1016/j.snb.2016.02.053.

[29] Y. Chen, Z. Yang, X.G Jia, Y.H. Wu, N.Y. Yuan, J.N. Ding, W.H. Zhang, S.Z. Liu, Thermally stable methylammonium-free inverted perovskite solar cells with Zn^{2+} doped $CuGaO_2$ as efficient mesoporous hole-transporting layer, Nano Energy 61 (2019) 148-157. https://doi.org/10.1016/j.nanoen.2019.04.042.

[30] Z. Xu, D.H. Xiong, H. Wang, W.J. Zhang, X.W. Zeng, L.Q. Ming, W. Chen, X.B. Xu, J. Cui, M.K. Wang, S. Powar, U. Bach, Y.B. Cheng, Remarkable photocurrent of p-type dye-sensitized solar cell achieved by size controlled $CuGaO_2$ nanoplates, J. Mater. Chem. A 2 (2014) 2968-2976. https://doi.org/10.1039/c3ta14072e.

[31] Y. Sun, F. Li, Z.C. Shen, Y.B. Li, J.X. Lang, W.M. Li, G.X. Gao, S.J. Ding, C.H. Xiao, T. Matsue, $NiCoO_2$@CMK-3 composite with nanosheets-mesoporous structure as an efficient oxygen reduction catalyst, Electrochim. Acta 294 (2019) 38-45. https://doi.org/10.1016/j.electacta.2018.10.060.

[32] J. Wang, B.B. Yang, H.W. Wang, P. Yang, Y.K. Du, Highly sensitive electrochemical determination of Sunset Yellow based on gold nanoparticles/graphene electrode, Anal. Chim. Acta 893 (2015) 41-48. https://doi.org/10.1016/j.aca.2015.08.042.

[33] G.F. Alves, L.V. de Faria, T.P. Lisboa, C.C. de Souza, B.L.M. Fernandes, M.A.C. Matos, R.C. Matos, A portable and affordable paper electrochemical platform for the simultaneous detection of sunset yellow and tartrazine in food beverages and desserts, Microchem. J. 181 (2022) 107799. https://doi.org/10.1016/j.microc.2022.107799.

[34] R. Darabi, M. Shabani-Nooshabadi, $NiFe_2O_4$-rGO/ionic liquid modified carbon paste electrode: An amplified electrochemical sensitive sensor for determination of Sunset Yellow in the presence of Tartrazine and Allura Red, Food Chem. 339 (2021) 127841. https://doi.org/10.1016/j.foodchem.2020.127841.

[35] M.L. Wang, J.W. Zhao, Facile synthesis of Au supported on ionic liquid functionalized reduced graphene oxide for simultaneous determination of Sunset yellow and Tartrazine in drinks, Sens. Actuators B Chem. 216 (2015) 578-585. https://doi.org/10.1016/j.snb.2015.04.053.

[36] H. Alp, D. Başkan, A. Yaşar, N. Yaylı, Ü. Ocak, M. Ocak, Simultaneous Determination of Sunset Yellow FCF, Allura Red AC, Quinoline Yellow WS, and Tartrazine in Food Samples by RP-HPLC, J. Chem. 2018 (2018) 1-6. https://doi.org/10.1155/2018/6486250.

[37] J.A. Rodriguez, I.S. Ibarra, J.M. Miranda, E. Barrado, E.M. Santos, Magnetic solid phase extraction based on fullerene and activated carbon adsorbents for determination of azo dyes in water samples by capillary electrophoresis, Anal. Methods 8 (2016) 8466-8473. https://doi.org/10.1039/C6AY02631A.

[38] P. Sierra-Rosales, C. Toledo-Neira, J.A. Squella, Electrochemical determination of food colorants in soft drinks using MWCNT-modified GCEs, Sens. Actuators B Chem. 240 (2017) 1257-1264. https://doi.org/10.1016/j.snb.2016.08.135.

[39] G. Figueira Alves, L. Vinícius de Faria, T. Pedrosa Lisboa, C. Cunha de Souza, B. Luiz Mendes Fernandes, M. Auxiliadora Costa Matos, R. Camargo Matos, A portable and affordable paper electrochemical platform for the simultaneous detection of sunset yellow and tartrazine in food beverages and desserts, Microchem. J. 181 (2022) 107799. https://doi.org/10.1016/j.microc.2022.107799.

[40] M.R. Majidi, R. Fadakar, B. Baj, A. Naseri, Carbon Nanotube-Ionic Liquid (CNT-IL) Nanocamposite Modified Sol-Gel Derived Carbon-Ceramic Electrode for Simultaneous Determination of Sunset Yellow and Tartrazine in Food Samples, Food Anal. Methods 6 (2013) 1388-1397. https://doi.org/10.1007/s12161-012-9556-6.

[41] L. Magerusan, F. Pogacean, M. Coros, C. Socaci, S. Pruneanu, C. Leostean, I.O. Pana, Green methodology for the preparation of chitosan/grapheme nanomaterial through electrochemical exfoliation and its applicability in Sunset Yellow detection, Electrochim. Acta 283 (2018) 578-589. https://doi.org/10.1016/j.electacta.2018.06.203.

[42] N. Nuñez-Dallos, M.A. Macías, O. García-Beltrán, J.A. Calderón, E. Nagles, J. Hurtado, Voltammetric determination of amaranth and tartrazine with a new double-stranded copper(I) helicate-single-walled carbon nanotube modified screen printed electrode, J. Electroanal. Chem. 822 (2018) 95-104. https://doi.org/10.1016/j.jelechem.2018.05.017.

[43] N.R. Barveen, T.J. Wang, Y.H. Chang, Z.Y. Liu, Ultrasensitive and reusable SERS probe for the detection of synthetic dyes in food industry through hybrid flower-shaped ZnO@Ag nanostructures, J. Alloy. Compd. 861 (2021) 157952. https://doi.org/10.1016/j.jallcom.2020.157952.

[44] K.Q. Deng, C.X. Li, X.F. Li, H.W. Huang, Simultaneous detection of sunset yellow and tartrazine using the nanohybrid of gold nanorods decorated graphene oxide, J. Electroanal. Chem. 780 (2016) 296-302. https://doi.org/10.1016/j.jelechem.2016.09.040.

[45] S. Ahmadi, M. Hasanzadeh, Z. Ghasempour, Sub-micro electrochemical recognition of carmoisine, sunset yellow, and tartrazine in fruit juices using P(β-CD/Arg)/CysA-AuNPs/AuE, Food Chem. 402 (2023) 134501. https://doi.org/10.1016/j.foodchem.2022.134501.